

Effect of High Cooling Rates on the Mineralogy and Hydraulic Properties of Stainless Steel Slags

LUBICA KRISKOVA, YIANNIS PONTIKES, LIEVEN PANDELAERS, ÖZLEM CIZER, PETER TOM JONES, KOEN VAN BALEN, and BART BLANPAIN

This article investigates the effect of chemical composition and cooling rate during solidification on the mineralogy and hydraulic properties of synthetic stainless steel slags. Three synthetic slags, covering the range of typical chemical composition in industrial practice, were subjected to high cooling rates, by melt spinning granulation or quenching in water, and to low cooling rates, by cooling inside the furnace. Both methods of rapid cooling led to volumetrically stable slags unlike the slow cooling which resulted in a powder-like material. Stabilized slags consisted predominantly of lamellar β -dicalcium silicate (β -C₂S) and Mg, Ca-silicates (merwinite and bredigite); the latter form the matrix at low basicity and are segregated along the C₂S grain boundaries at high basicities. Slowly cooled slags consist of the γ -C₂S polymorph instead of the β -C₂S and of less Mg, Ca-silicates. Isothermal conduction calorimetry and thermogravimetric analysis indicate the occurrence of hydration reactions in the stabilized slags after mixing with water, while calcium silicate hydrates (C-S-H) of typical acicular morphology are identified by SEM. The present results demonstrate that the application of high cooling rates can result in a stable, environmental-friendly, hydraulic binder from stainless steel slags, rich in β -C₂S, without the necessity of introducing any additions to arrest the β polymorph.

DOI: 10.1007/s11663-013-9894-9

© The Minerals, Metals & Materials Society and ASM International 2013

I. INTRODUCTION

THE most common stainless steel making process consists of the following steps: (i) melting of scrap and alloys in an electric arc furnace (EAF), (ii) carbon and sulphur removal and adjustment of the steel chemical composition during argon oxygen decarburization (AOD), followed by (iii) final alloying, homogenization and removal of inclusions in the ladle metallurgy (LM).^[1] In all these processes, a large amount of slag is generated. Mainly the last two slags, AOD and LM slags, are the slags with high basicity (*i.e.*, high CaO/SiO₂ ratio). Although the chemical composition of these slags can vary to some extent, both consist mainly of Ca, Si, and Mg. The main minerals typically found in these slags are dicalcium silicate (Ca₂SiO₄), merwinite (Ca₃MgSi₂O₈), bredigite (Ca₇MgSi₄O₁₆), and periclase (MgO).^[2]

Dicalcium silicate (C₂S) occurs in several polymorphic forms: α , α'_H , α'_L , β and γ . Most of these are stable in the pure state only at elevated temperatures and it is merely the γ form that is stable at room temperature. The β -to- γ phase transition is an athermal, displacive transformation^[3] which involves a rotation of the SiO₄ tetrahedra and large movements of calcium atoms.^[4] It is accompanied with a volume increase of 12 pct causing a disintegration into small particles, a phenomenon known as “dusting”.^[5,6] Apart from potentially too high Cr contents, dusting, which is frequently observed during cooling and occasionally during subsequent storage of the slag, is one of the main impediments for stainless steel slag valorization on an industrial scale. Thus, the prevention of such disintegration has been one of the major issues in the stainless steel slag processing for a considerable time.^[7]

Several methods have been suggested so far to stabilize the β -C₂S (or other high temperature polymorphs) and thus avoid slag disintegration. Principally, these methods can be divided into two groups; chemical stabilization and physical stabilization. Chemical stabilization (*e.g.*, by boron addition) has been studied extensively and several predictions have been made about which ions can stabilize β -C₂S.^[8,9] These predictions are based on the ionic radius (R), charge to ionic radius ratio (C/R), and ion polarization ability (C^2/R).^[7,9] On the other hand, physical stabilization of the metastable high temperature polymorph can be obtained when the “free standing” particles are below a critical size.^[6,9] The effect of grain size has been studied in zirconia composite ceramics, for which only particles of a critical size range (R_c) were capable of undergoing a

LUBICA KRISKOVA, Ph.D. Student, YIANNIS PONTIKES and LIEVEN PANDELAERS, Dr. Engineering Researchers, PETER TOM JONES, Dr. Engineering Research Manager, and BART BLANPAIN, Professor, are with the High Temperature Processes and Industrial Ecology Research Group, Department of Metallurgy and Materials Engineering, KU Leuven, Kasteelpark Arenberg 44, 3001 Leuven, Belgium. Contact e-mail: yiannis.pontikes@mtm.kuleuven.be ÖZLEM CIZER, Dr. Researcher, is with the High Temperature Processes and Industrial Ecology Research Group, Department of Metallurgy and Materials Engineering, KU Leuven, and also with the Building Materials and Building Technology Division, Department of Civil Engineering, KU Leuven, Kasteelpark Arenberg 40, 3001 Leuven, Belgium. KOEN VAN BALEN, Professor, is with the Building Materials and Building Technology Division, Department of Civil Engineering, KU Leuven.

Manuscript submitted October 24, 2012.

Article published online June 26, 2013.

crack-tip, stress-induced, martensitic transformation. The critical volume of a particle was derived from the overall particle size or the twin dimension, which in this case would relate to the α' -to- β transformation.^[6] The particle size can be controlled by an external influence on the grains, *e.g.*, by solidifying under specific cooling rates.^[6,9,10]

Rapid cooling can be used for slag amorphization or encapsulation of metals and oxides in their structure.^[11] Granulation, being one of the rapid cooling methods, is an established method industrially used in blast furnace slag processing and produces an amorphous material with hydraulic potential, *i.e.*, ground-granulated blast furnace slag.^[12] Besides blast furnace slag, Tossavainen *et al.*^[11] stabilized LM slag by amorphization through water granulation, whereas Li^[13] reported that the granulation of BOF slag is an efficient method for its volume stabilization (no free lime and magnesia) as well as heat recovery. It is therefore conceivable to suggest rapid cooling also for stainless steel slag, provided the end product is of higher value.

For very slow cooling rates, computational thermodynamics^[14] and Scheil–Gulliver modeling^[15] are able to reasonably predict slag mineralogy. Experimentally, differential scanning calorimetry (DSC) can be used to detect the onset of crystallization;^[16] however, lab instruments cannot achieve high cooling rates. Confocal scanning laser microscopy (CSLM) coupled with a high temperature furnace^[17] and the hot thermocouple technique are alternatives, the latter being able to offer cooling rates of the order of 400 K/s.^[18] High cooling rates, applied for the synthesis of special glasses, allow for little processing control, and conclusions are usually deduced post mortem.^[19] Indeed, for the experimental approach followed in the current study, the cooling rates achieved are expected to be higher than 400 K/s. Moreover, due to the high basicity of the slag studied, unlike blast furnace compositions, the solidified slag is crystalline, whereas some of the transformations occurring are very difficult to be detected, *e.g.*, the $\beta \rightarrow \gamma$ C₂S conversion is athermal. To this extent, the development of TTT or CTT diagrams is practically very difficult.

Despite the above challenges, it is of great interest to investigate if the β -C₂S phase in the stainless steel slags of high basicity (CaO/SiO₂) can be stabilized *via* rapid cooling. If successfully established, this would imply that stainless steel slags can indeed be valorized in higher added-value applications with respect to the current

main industrial use, namely as aggregates in asphalt applications. Two methods of rapid cooling, *i.e.*, one of granulation by means of melt spinning and water quenching, and the other method using slow cooling were adopted. The effects of these cooling paths on the mineral composition of the slags are investigated by means of quantitative X-ray diffraction analysis and then compared with FactSage calculations. Ultimately, the hydraulic potential of the solidified slags is assessed and an outlook toward industrial scale valorization is given.

II. MATERIALS AND METHODS

Synthetic slags with three different compositions comparable to AOD and LM slags were prepared by mixing analytic grade oxides/carbonates, Table I. The various basicities (CaO/SiO₂) were chosen to cover the whole range of chemical compositions of typical AOD and LM slags. Indeed, this is the drive behind using synthetic slags, that is, the ability to control the ratio CaO/SiO₂ without any other changes in slag chemistry. This would have not been possible with industrial slags where the chemical composition varies from batch to batch. To ensure the homogeneity of the synthetic slag mixtures, the mixing was performed in an ethanol suspension for 6 hours. After drying, the mixtures were heated up to 1173 K (900 °C) for 3 hours to remove the carbonates.

The rapid cooling was performed in an induction-heating set-up using graphite crucibles. Approximately 20 g of slag mixture was introduced into the crucible for each experiment. The heating cycle was RT to 1973 K \pm 30 K (1700 °C \pm -243 °C) within 7 minutes in, followed by an isothermal step at this temperature for an additional 7 minutes to homogenize the melt. The molten slag was released from the crucible by raising the graphite pin blocking the orifice at the bottom of the crucible. The melt was either granulated on a rotating copper wheel (G) or quenched in water (WQ). Both rapid cooling methods were performed in a protective argon atmosphere. The rapidly cooled slags were collected and the fraction >250 μ m was used; the rest was considered disintegrated. The solidified slags were milled in a planetary ball mill (Retsch, PM4) for 1 hour at 200 rpm by using 5-mm stainless steel milling balls. The

Table I. Chemical Composition of Synthetic Slags and Typical Compositions of Argon Oxygen Decarburization Slag (AOD) and Ladle Metallurgy Slag (LM), in Weight Percentage

Chemical Formula	Chemical Composition				
	I	II	III	AOD	LM
CaO	52.4	54.7	56.7	45 to 60	50 to 70
SiO ₂	32.7	30.4	28.4	30 to 40	15 to 25
MgO	6.5	6.5	6.5	5 to 12	0 to 10
Al ₂ O ₃	1.3	1.3	1.3	<5	<1
TiO ₂	1.1	1.1	1.1	~1	~1
CaF ₂	6.0	6.0	6.0	4 to 6	8 to 12
Basicity	1.6	1.8	2.0	~1.6	>1.6

particle size distribution of finely milled slags was determined by laser scattering (MasterSizer Micro Plus, Malvern). As a reference for comparison, slag samples were also subjected to slow cooling. For this purpose, approximately 20 g of slag was heated up to 1903 K (1630 °C) in a bottom loading furnace (AGNI ELT 160-02), under static atmosphere, held for 2 hours, and cooled down to RT at 5 K/min. A Pt crucible was used for the slow cooling experiments.

In order to estimate the cooling rate of the granulated slag (G), a numerical 1D model, Figures 1 through 4, was used to simulate the slag cooling during the first 15 seconds after granulation on the drum.^[20]

The transient temperature evolution over the thickness of an infinitely wide slag ribbon was calculated by solving the heat-transport equation, with r being the spatial coordinate, T the temperature, k the thermal conductivity, and H the volumetric enthalpy:

$$r \frac{\partial H}{\partial t} = \frac{\partial}{\partial r} \left(rk \frac{\partial T}{\partial r} \right) \quad [1]$$

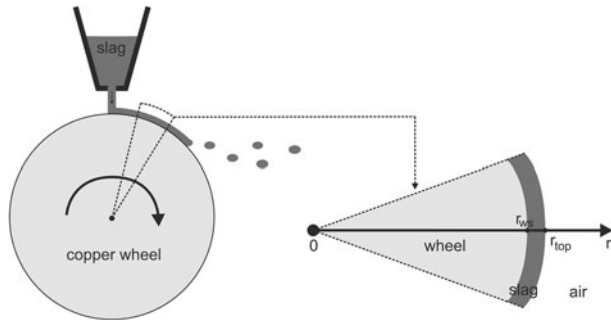


Fig. 1—Schematic of the modeled cylindrical ID geometry. A slag layer with thickness ($r_{top} - r_{ws}$) makes contact with a copper wheel with radius r_{ws} and cools by conduction to the wheel and by convection to the surrounding air. A pie-shaped part of the wheel is shown for illustration.

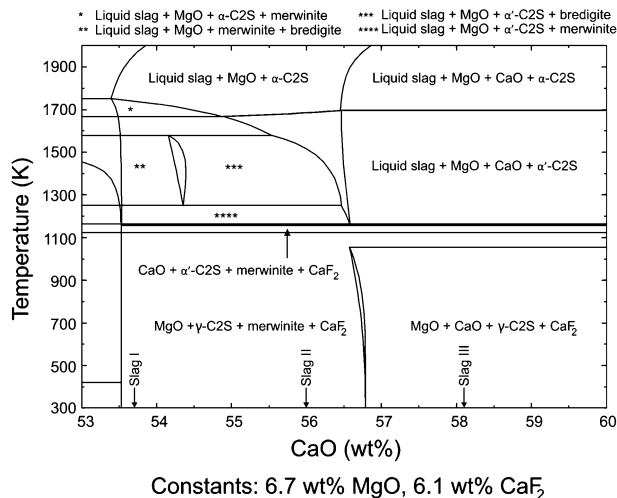


Fig. 2—Section of the isoplethal phase diagram CaO-SiO₂ at constant MgO and CaF₂ content.

Two periods are distinguished. During the first 0.2 seconds, the slag makes contact with the drum at one side and the air at the other, to undergo cooling by conduction and combined convection and radiation, respectively. The respective boundary conditions at the wheel–slag (r_{ws}) and the slag–air (r_{top}) interfaces are

$$k_{wheel} \left(\frac{\partial T_{wheel}}{\partial r} \right)_{r=r_{ws}} = k_{slag} \left(\frac{\partial T_{slag}}{\partial r} \right)_{r=r_{ws}} \quad [2]$$

$$k_{slag} \left(\frac{\partial T}{\partial r} \right)_{r=r_{top}} = h(T_{air} - T_{top}) + \sigma \epsilon (T_{air}^4 - T_{top}^4) \quad [3]$$

with h being the convection coefficient for the air, $\epsilon = 0.8$ the emissivity, and σ the Stefan–Boltzmann constant.

In the remainder of the time, the slag was assumed to contact air at both sides, and to cool by convection only. The subsequent collection of the particles on a metal plate was not considered explicitly, as the most important transformation was assumed to happen during these two periods. During the free flight phase, the wheel–slag boundary becomes a new external boundary, and the boundary condition is replaced by one of the second kind. If the radiation term is omitted from Eq. [3], this boundary condition can also be used to simulate the water quenching of the slag, where h represents the heat-transfer coefficient for water:

$$k_{slag} \left(\frac{\partial T}{\partial r} \right)_{r=r_{top}} = h(T_{air} - T_{top}) \quad [4]$$

For all calculations, the temperature- and composition-dependent enthalpy was determined using FactSage 6.1 (Thermfact/CRCT, Montreal, Canada and GTT-Technologies, Aachen, Germany). The thermal conductivity of the slag was fixed at 1.5 W/(mK), and the heat-transfer coefficient at the slag–air interface was 50 W/(m²K), a representative value for moving air, while, for simulating water quenching, h was assumed as 1000 W/(m²K).^[21]

The mineralogy of the materials was determined by X-ray powder diffraction analysis (XRPD, D500 Siemens). Diffraction patterns were measured in 2θ range of 10 to 70 deg using Cu K α radiation of 40 kV and 40 mA, with a 0.02 deg step size and step time of 4 seconds. Rietveld quantitative phase analysis was performed using the “Topas[®] Academic” software.

The effect of the rapid cooling on the mineralogy was evaluated by comparing the measured observed phases with the expected mineralogy according to FactSage calculations. The FactPS and FToxid databases were used, and two cases were considered: equilibrium, and Scheil–Gulliver solidification. In equilibrium solidification, it is assumed that diffusion is infinitely fast and that the entire system is in global equilibrium. These conditions are typical for very slow cooling processes. In Scheil–Gulliver solidification, there is no diffusion or transformation in the solid phases. This means that all solid phases remain as solidified. This behavior is

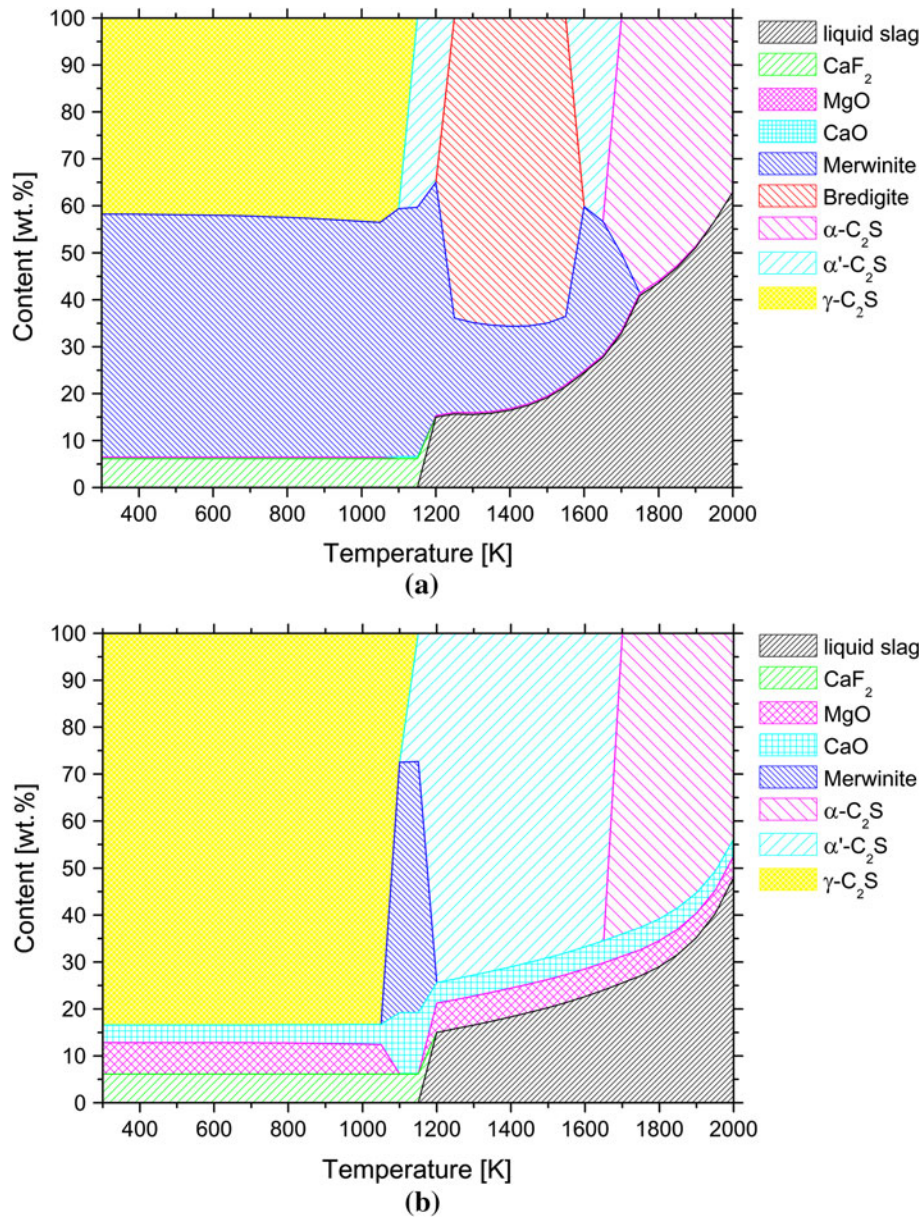


Fig. 3—FactStage thermodynamic calculations based on equilibrium cooling for slag (a) I and (b) III.

expected for very fast cooling. Real solidification problems are typically situated in between these two extreme scenarios.^[22]

The microstructural characterization of stabilized granulated and water-quenched slags was performed using a scanning electron microscopy (SEM XL30, Philips). For this purpose, the embedded materials were prepared using a standard sample preparation method and etched in 3 vol pct Nital for 5 seconds. Wavelength dispersive spectroscopy (WDS) was used for chemical composition mapping on the granulated polished samples by using an accelerating voltage of 20 kV (JXA-8530F, JEOL). The average grain size was estimated based on measurements performed using ImageJ software. In each sample, C_2S grains ranging from 50 to 100 were measured, and the average value is reported.

The hydraulic reactions were monitored using isothermal conduction calorimetry (TAM Air device, TA Instruments) at 293 K (20 °C). The analyses were performed on pastes with a water-to-solid ratio (w/s) of 0.75. Furthermore, the paste samples were stored in sealed plastic capsules for 3, 7 and 28 days. After the designated period of time, the samples were crushed to powder and the hydration was stopped by vacuum-drying (Alpha 1-2 LD, Martin Christ) for 2 hours at 0.035 mbar. Powder samples were subjected to thermal analysis using simultaneous TGA/DSC (STA 409 PC Luxx[®], Netzsch). The samples were heated at 5 K/min in a continuous N_2 flow up to 1273 K (1000 °C). Bulk samples were used for the microstructural characterization of hydrated products using a scanning electron microscope (SEM XL30, Philips). To avoid structural

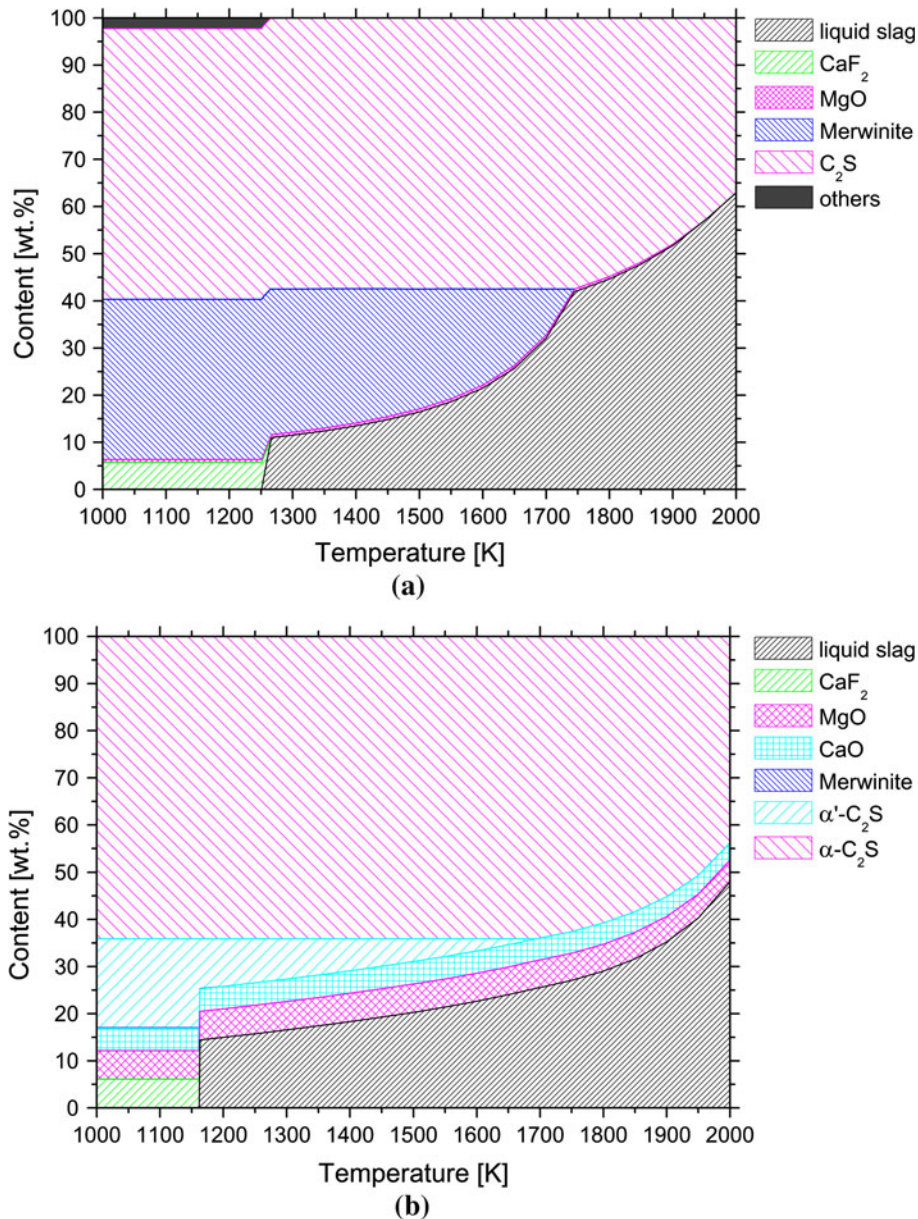


Fig. 4—FactSage thermodynamic calculations based on a Scheil–Gulliver cooling model for slag (a) I and (b) III.

destruction of the hydrated phases during drying, bulk paste samples were kept in an oven at 323 K (50 °C) for 2 days.

III. RESULTS AND DISCUSSION

A. Slow Cooling

All studied slags were basic with a CaO/SiO₂ (C/S) mass ratio higher than 1, and as expected, slow cooling resulted in a fully powdered form of material because of the β to γ phase transformation of C₂S during cooling. The increase in C/S from sample I to III is reflected in the mineralogy, as shown by the Rietveld analyses of the slowly (furnace) cooled slags in Table II. The amount of

Table II. XRD Determined and Mineralogical Composition of Slowly (Furnace) Cooled Slags, in Weight Percentage

Mineral Phase	Chemical Formula	Cooling [5 K/min (5 °C/min)]		
		I	II	III
β-C ₂ S	Ca ₂ SiO ₄	2	4	5
γ-C ₂ S	Ca ₂ SiO ₄	49	72	75
Periclase	MgO	<1	6	8
Merwinite	Ca ₃ MgSi ₂ O ₈	26	5	4
Bredigite	Ca ₇ MgSi ₄ O ₁₆	5	5	<1
Fluorite	CaF ₂	<1	4	5
Cuspidine	Ca ₄ Si ₂ F ₂ O ₇	14	2	3
Wollastonite	CaSiO ₃	2	2	1

γ -C₂S increased for higher C/S ratios, amounting to over 70 wt pct in samples II and III. In sample I, the lower γ -C₂S (Ca₂SiO₄) content was counterbalanced by an approximately equally higher merwinite (Ca₃MgSi₂O₈) content. Other minor phases were bredigite (Ca₇MgSi₄O₁₆), MgO, β -C₂S (Ca₂SiO₄), and wollastonite (CaSiO₃). F was mainly present in CaF₂, for samples II and III, or cuspidine (Ca₄Si₂F₂O₇), for sample I.

The evaluation of the mineralogy could be interpreted by comparing with the calculated isoplethal section in Figure 2 in conjunction with the calculated cooling paths in Figures 3 and 4, for equilibrium and Scheil–Gulliver conditions, respectively. To simplify the calculations, a four-component system consisting of CaO, SiO₂, MgO, and CaF₂ was considered, neglecting the small amounts of TiO₂ and Al₂O₃ that have only little influence on the mineralogy. While the phase diagram section allows one to easily visualize which phases are present as a function of temperature, the cooling calculations quantify the amounts of the stable phases.

As expected for slowly cooled samples, the quantitative XRD data agreed best with the equilibrium calculations. The model results reproduced the decrease in merwinite and the accompanied increase in γ -C₂S content for sample III compared with I. For sample I, merwinite precipitated from the melt at high temperature and remained stable throughout the entire cooling trajectory down to room temperature. Bredigite was also formed, at the expense of merwinite and α' -C₂S, but was stable only between 1579 K and 1249 K (1306 °C and 976 °C). In slag II, bredigite formed at 1500 K (1227 °C) but was also only stable until 1249 K (976 °C). The presence of some remaining bredigite in the RT microstructure indicates that the experimental conditions slightly deviate from equilibrium. For slag III, one of the first solid phases to form was MgO, which remained stable until room temperature in agreement with the experimental data for slow cooling. In contrast to samples I and II, bredigite was not formed in slag III, and the merwinite stability range was limited from 1156 K to 1053 K (883 °C to 780 °C), explaining the very low measured quantities. In nearly all cases, the model predicted no cuspidine but expected all F to be present as CaF₂. Only for the cooling under Scheil–Gulliver conditions, a small amount of cuspidine was predicted for slag I. Overall, the equilibrium cooling model and analytic data on the mineral composition agreed well both qualitatively and semi-quantitatively.

Due to the assumption of no solid-state transformations under Scheil–Gulliver conditions, the mineralogy predicted for the Scheil–Gulliver model contained no γ -C₂S but high temperature polymorphs. If it is assumed that these would still transform to γ -C₂S, the mineralogy at room temperature would be qualitatively similar to the one from equilibrium calculations.

B. Rapid Cooling

1. Cooling rate model

The quenching experiments showed that the (wall) thickness of the stabilized slag was typically around 1 mm. Based on this, the calculations of the temperature

evolution in the slag during cooling, although simplifying the reality, can give an indication of the cooling speed required for stabilization.

First, the granulation on a copper drum was considered. Figure 5(a) shows the calculated temperature evolution as a function of time at three positions in a 1-mm slag ribbon with composition III. Initially, the slag that contacted the wheel cooled very fast, whereas the air side of the slag cooled slower. When the slag left the wheel, the cold end heated up again, as heat was conducted to it from the hotter part of the ribbon. This reheating could be reduced by improving the heat transfer, for instance, by water spraying ($h \sim 1000$ W/(m²K)). Another way to enhance the cooling would be by reducing the ribbon thickness, as illustrated in Figure 5(b). Very thin ribbons with a thickness of 0.25 mm were quenched up to 473 K (200 °C) in a fraction of a second. The average cooling rate dropped quickly as thickness increased. For a 1-mm ribbon, there was still an initial slope in temperature, whereas such a slope was hardly observed for a 3-mm ribbon. Simulations have also been run for compositions I and II. If the composition dependent enthalpy was taken as the only variable, no significant effect of the slag composition on the cooling behavior was observed.

The second case constitutes slag quenching in water. Figure 6 shows the evolution of the average temperature

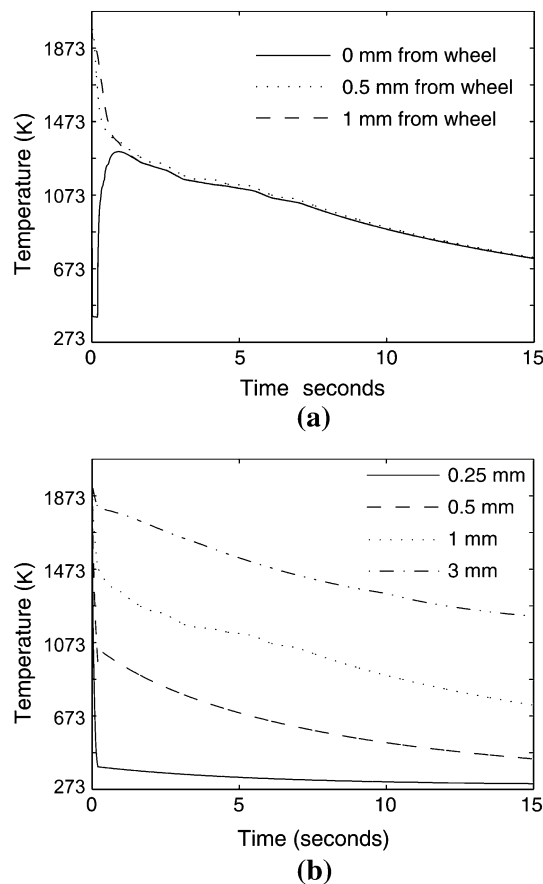


Fig. 5—Calculated temperatures for the granulation of a slag ribbon. (a) Temperature profile at three different positions in a 1-mm-thick slag ribbon. (b) Average temperature for four ribbon thickness.

in this case for a ribbon and a sphere. Compared with the cooling on a copper drum, the cooling is slower during the first 0.2 seconds, *i.e.*, the time during which the slag contacts the drum. However, because water was a much more efficient cooling medium than air, the average temperature kept dropping at a faster rate compared with cooling on the drum. Consequentially, for a 1-mm ribbon, the average temperature in the slag reached room temperature faster than in the granulation case. This observation may be linked to the relative amounts of β -C₂S and γ -C₂S as shown in Table III: the faster overall cooling when quenching in water led to a higher amount of β -C₂S and thus a larger stabilized fraction. Even faster cooling could be obtained for a spherical geometry.

Nonetheless, it should be acknowledged that it is the thickness of the solidifying material which is the most crucial parameter affecting cooling rate. It is therefore believed that once the thickness of the granules is controlled and kept small enough, the cooling rate and resulting stabilization ability could be similar or even better for melt spinning granulation compared with water quenching.

2. Physical properties

Slags granulated by melt spinning resulted in spherical, hollow spherical and ribbon-like morphologies, Figure 7(a). The maximum diameter of hollow spherical

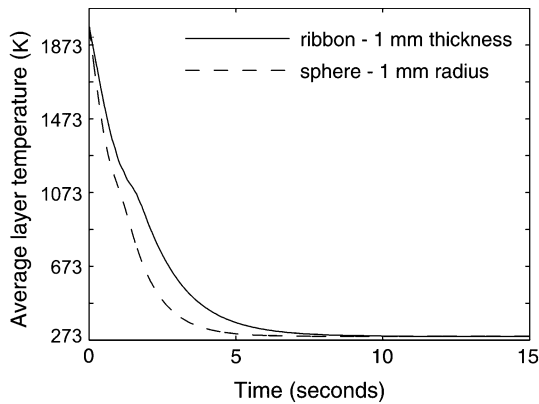


Fig. 6—Calculated average temperature in water-quenched slags for a 1-mm ribbon and a sphere of 1-mm radius.

Table III. XRD Determined Mineralogy of Slags Subjected to Granulation (G) and Water Quenching (WQ), in Weight Percentage

Mineral Phase	Chemical Formula	I		II		III	
		G	WQ	G	WQ	G	WQ
β -C ₂ S	Ca ₂ SiO ₄	7	19	21	29	68	82
γ -C ₂ S	Ca ₂ SiO ₄	—	—	20	10	19	4
Merwinite	Ca ₃ MgSi ₂ O ₈	42	43	9	5	—	—
Bredigite	Ca ₇ MgSi ₄ O ₁₆	44	35	41	49	<1	4
Fluorite	CaF ₂	2	2	4	4	5	3
Cuspidine	Ca ₄ Si ₂ F ₂ O ₇	5	<1	—	—	—	—
Periclase	MgO	—	—	5	3	8	7

granules was below 1 cm. However, the thickness of their walls was comparable to the maximum thickness of stabilized ribbon-like slags, *i.e.*, 1 mm approximately. Water quenching resulted in a volumetrically stable, brittle and porous product, occasionally larger than 4 cm, Figure 7(b). The shell of the granules was thin, typically much less than 1 mm.

Interestingly, a part of the rapidly cooled slags disintegrated in the following days. This phenomenon, known as late falling,^[23] was more pronounced on slags with lower-basicity. As the cooling model did not reveal any difference in the cooling behavior related to the slag composition, this feature may be connected to the slag viscosity. According to a calculation based on Riboud's model, the viscosity of slag I was found to be almost two times the viscosity of slag III at 1896 K (1623 °C). Corresponding to this calculation, the granulation of slag I resulted in granules and strips appearing to be thicker compared with granules of slag III. As discussed previously, thickness is the main parameter influencing

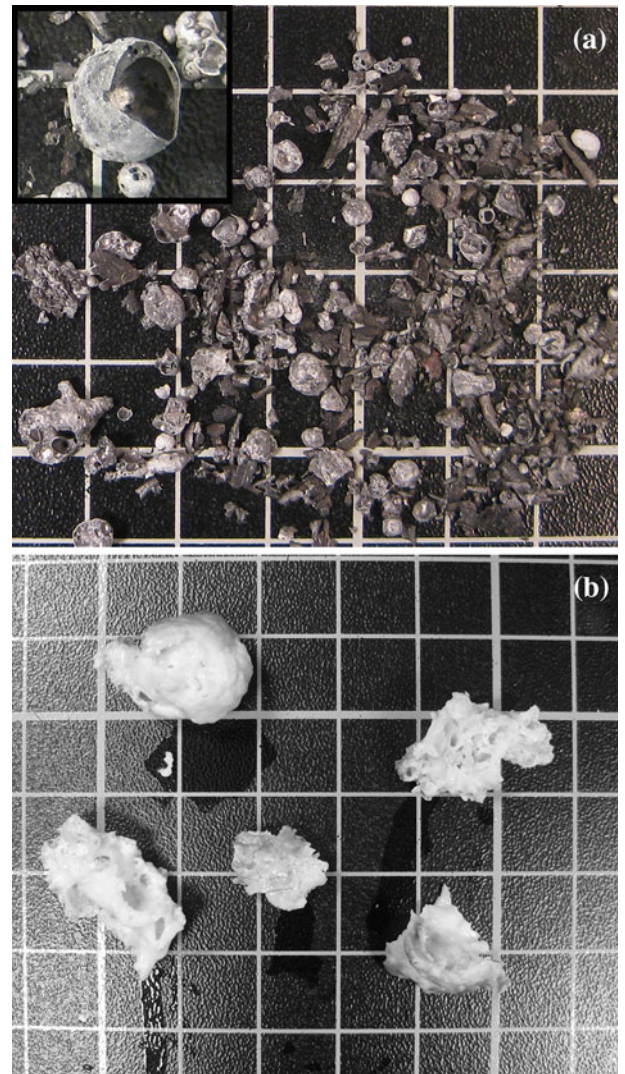


Fig. 7—Stabilized slag after (a) granulation, (b) water quenching, mesh dimension is 1 cm.

the cooling rate and the resulting stabilization effectiveness. To that extent, the more pronounced late falling of slags with low basicity could be linked to the higher thickness of produced granules and the slower cooling rate during solidification.

3. Mineralogy

The mineralogy after cooling for both types of rapid cooling techniques consisted of bredigite, merwinite and C_2S polymorphs as the major phases (Table III). Similarly to the furnace cooled slags, the amount of total C_2S increased at higher basicity at the expense of merwinite and bredigite, whereas Mg was mostly present in the form of periclase (MgO) at higher basicities. The mineralogical composition of both granulated and water-quenched slags was qualitatively comparable. However, the ratio β to γ - C_2S was higher for water-quenched samples compared with the granulated ones. This is most probably due to faster cooling during water quenching, as the cooling model has shown (Figures 5 and 6). Still, the evolution of mineralogy with increasing basicity represented a similar trend for both cooling methods indicating that the main factor was the chemical composition.

The calculations can help us here in interpreting how the mineralogy developed during cooling. For the slag with the highest basicity, slag III, the predicted RT mineralogy under equilibrium and Scheil–Gulliver conditions (Table IV) agree reasonably well with the XRD results (Tables II, III). However, to link the model output with the experimental data for slags I and II a more pragmatic approach is required. At RT, the calculations predict no bredigite, whereas XRD analysis reveals this as a major constituent with more than 40 wt pct in both slags. It thus appears that the bredigite, which is only stable in a limited temperature range, was effectively frozen into the microstructure. This means that the fast cooling conditions may allow for the formation of bredigite by the reaction of merwinite and C_2S ,^[24] but kinetically impede its decomposition at a lower temperature. This reasoning is further supported by the observation that in the furnace-cooled samples also, some traces of bredigite remained at room temperature. When comparing the experimental microstructure with the calculated mineralogy under equilibrium conditions at 3713 K and 1300 K (100 °C and 1027 °C), it is clear that the latter

lies more close to the measurements (Table IV) for slag I and slag II. In fact, the experimental data suggest that the decomposition of bredigite was only partially inhibited and that a fraction did transform to merwinite and C_2S .

Another factor that may affect the difference between experimental and calculated data is the fact that only stabilized material was analyzed. This could have introduced certain variation in the mineralogical composition as the disintegrated material (<250 μ m) may have a slightly different mineralogical composition, as evidenced by a small deviation in the chemical composition of rapidly cooled slags from the original composition. This factor could, for instance, explain the relatively high bredigite content in quickly cooled slag II, as well as the traces of bredigite in quickly cooled slag III, whereas this phase is not expected at all at the latter's composition.

4. Microstructural and microchemical analyses

Secondary electron (SE) micrographs of G are shown in Figures 8(a) through (c). At low basicities, β - C_2S solidified into egg-shaped nodules with a lamellar structure, resembling belite grains which are typically found in cement clinker. The typical lamellar structure of β - C_2S resulted from the twinning along {100} and/or {001} lattice planes, which occurred when a higher-temperature polymorph of C_2S transforms into β - C_2S on cooling.^[25] The structure of sample I-G consisted also of merwinite and bredigite, which were present in the matrix in the form of angular, randomly distributed grains, Figure 8(a). As the basicity increased, β - C_2S became the main phase constituting now more of the matrix, Figure 8(b). Other phases as merwinite, bredigite, and fluorite were randomly distributed in the structure in the shapeless grain form. Regarding sample III-G, the β - C_2S grains had an irregular shape, rather than an oval one, Figure 8(c). Merwinite, bredigite were identified as phases located at the grain boundaries forming a network. Dendrites, rich in magnesium were also periodically present in the structure. However, their compositions did not resemble the stoichiometry of any identified phase.

The structure of water-quenched (WQ) (Figure 9) slag sample looked similar to the granulated ones when the basicity was low. Large egg-shaped C_2S grains were randomly distributed in the merwinite–bredigite matrix,

Table IV. Calculated Mineralogical Composition of Slags Using Equilibrium and Scheil–Gulliver Model, in Weight Percentage

Mineral Phase	Chemical Formula	Equilibrium Cooling [373 K (100 °C)]			Scheil–Gulliver Cooling		
		I	II	III	I	II	III
CaO	CaO	—	—	4	—	—	5
C_2S	Ca_2SiO_4	42	77	83	57	85	83
Periclase	MgO	<1	5	6	1	5	6
Merwinite	$Ca_3MgSi_2O_8$	52	12	—	34	0.2	—
Bredigite	$Ca_7MgSi_4O_{16}$	—	—	—	—	3	—
Fluorite	CaF_2	6	6	6	6	6	6
Others		—	—	—	2	—	—

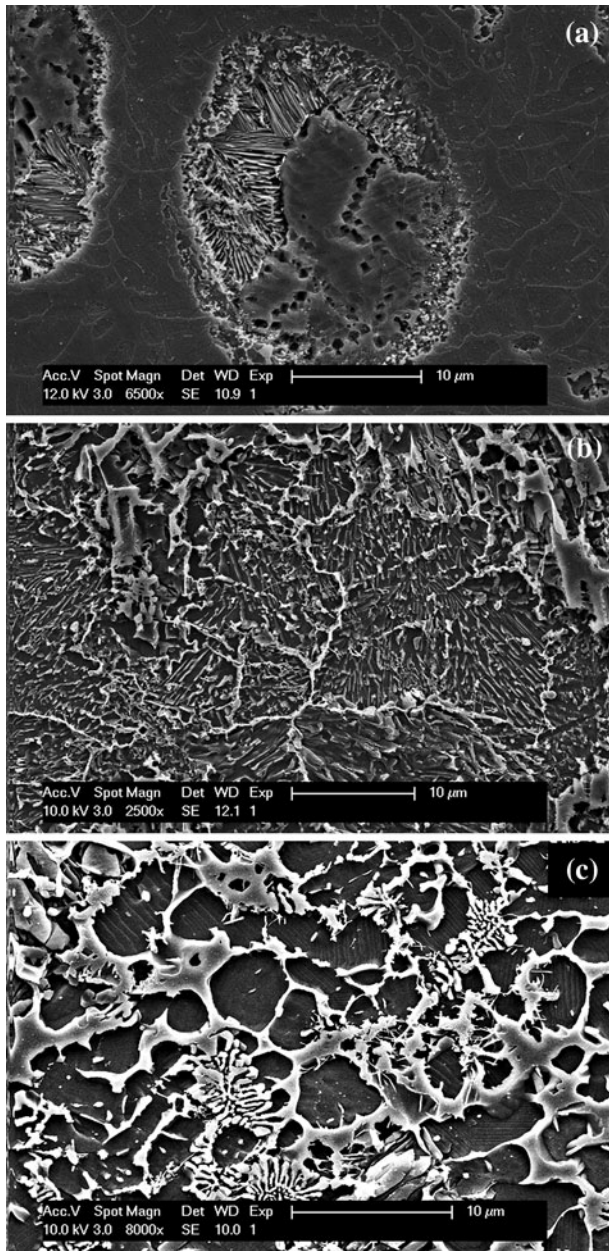


Fig. 8—SE-micrographs of slag stabilized of by granulation (a) I-G, (b) II-G (c) III-G.

Figure 9(a). However, at higher basicity, the structure of WQ samples contained more dendrites compared with granulated samples. Similarly, these dendrites were rich in magnesium not resembling the stoichiometry of any identified phase, Figure 9(b). At the highest basicity, the C_2S grains were present preserving their typical oval shape, Figure 9(c). A network of shapeless grains and dendrites was visible, similar to the sample II-WQ.

The average grain size of C_2S grains was measured on G samples. Even though the variation in grain size within one sample is considerable, a clear trend could be observed. The average C_2S grain size decreased from $19\ \mu\text{m}$ in sample I to approximately $3\ \mu\text{m}$ in sample III. The grain size in sample I was much higher than the critical particles size of $10\ \mu\text{m}$ reported by Chan *et al.*,^[6]

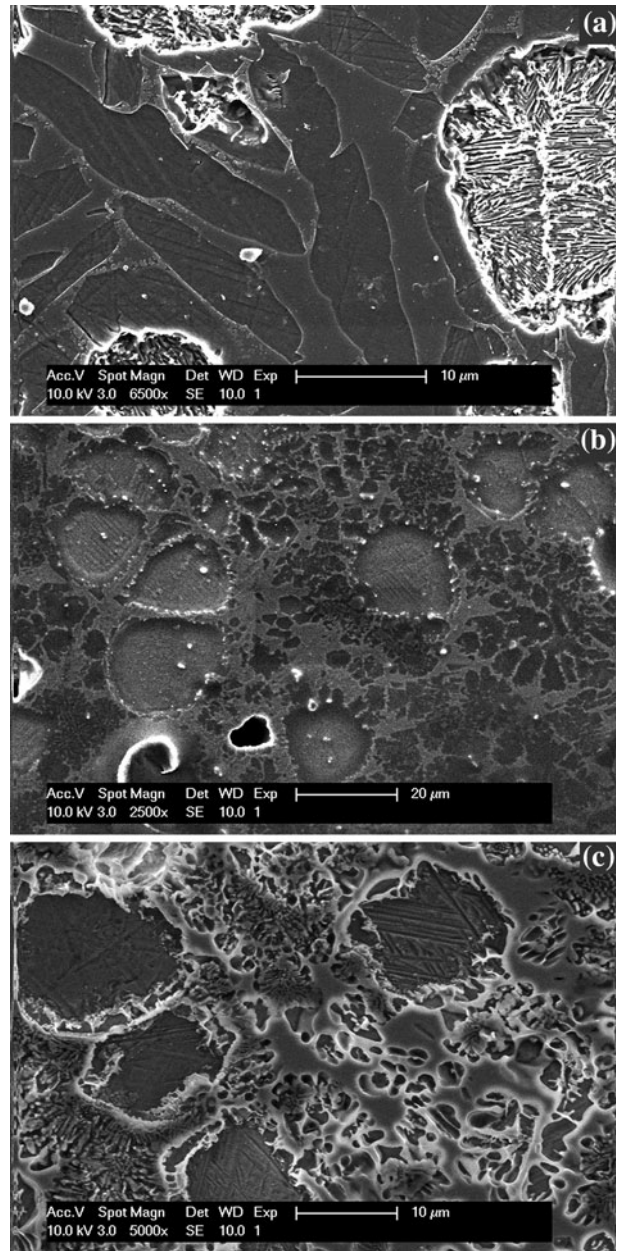


Fig. 9—SE micrographs of slag stabilized by water quenching (a) I-WQ, (b) II-WQ, and (c) III-WQ.

but as illustrated in Figures 8(a) and 9(a), the egg-shaped C_2S grains consisted of several sub-grains, and thus, the real grain size could be lower. Conversely, the larger grain size may be the reason for the significant delayed disintegration of rapidly cooled slag with lower basicity. As the slowly cooled slag disintegrated completely during cooling and the amount of stabilized $\beta\text{-}C_2S$ is relatively low, chemical stabilization did not play a crucial role.

Wavelength dispersive X-ray spectroscopy was performed to map the elemental distributions in the structure and the different phases. Figure 10 shows the elemental mappings of Ca, Si, Mg, Ti, Al, and F in granulated sample II-G. Two distinct areas were identified based on the mapping: rounded grains containing

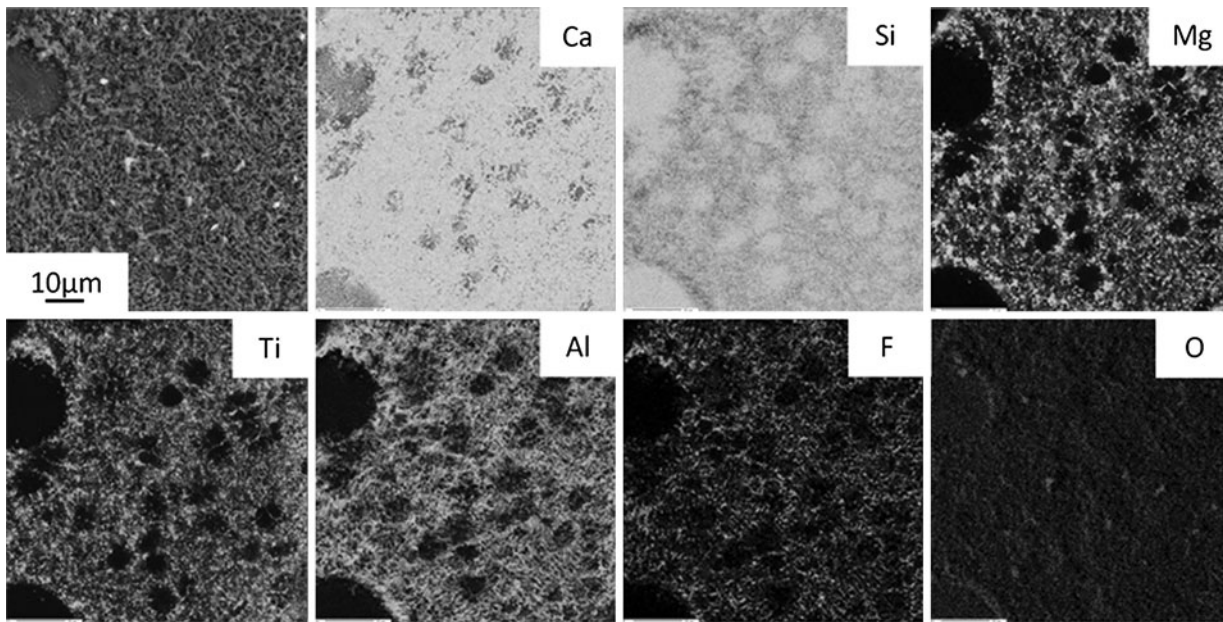


Fig. 10—Distribution of elements according to WDS in the granulated slag II-G.

Ca, Si, and oxygen only, and the matrix where all elements were randomly distributed. The Ca-Si-containing grains have been identified as C_2S . The matrix contained more Ca and less Si compared with C_2S and consisted of all other phases like merwinite, bredigite, fluorite, and cuspidine. Aluminum and Ti are according to^[26–29] common impurities in merwinite and bredigite, and were incorporated in their structure rather than precipitating as separate phases.

At higher magnification, it was revealed that the matrix is formed by at least two distinct features: the irregularly shaped grains containing mostly Ca and Si, and the along-the-grain-boundaries network of phases containing all other elements. The Ca-Si-rich areas contained traces of Ti, Al, and Mg as well and are believed to be the β - C_2S grains. As has been assumed elsewhere,^[8] all Ti^{4+} , Al^{3+} , and Mg^{2+} are dopant ions which can substitute either Ca or Si in the structure of the β - C_2S . Nonetheless, these ions are not expected to chemically stabilize β - C_2S .^[30,31]

5. Hydraulic properties

As the mineralogical compositions of both granulated and water-quenched slags were comparable, only granulated material was studied for hydraulic properties. Furnace-cooled slags were not studied for hydraulic properties as, being based on their mineralogy, the reactivity would be low. All finely milled slags (with d_{50} around 10 μm), besides sample I-G, showed reactivity when mixed with water, as demonstrated by the exothermic peaks in the calorimetric measurement, Figure 11. Both samples II-G and III-G showed two peaks, an initial small peak followed by a substantially larger exothermic peak. As has been reported elsewhere,^[32] approximately 5 to 15 wt pct of C_2S reacts during the first day of hydration. Based on this, the small peaks at 15 and 25 hours for slags III-G and II-G,

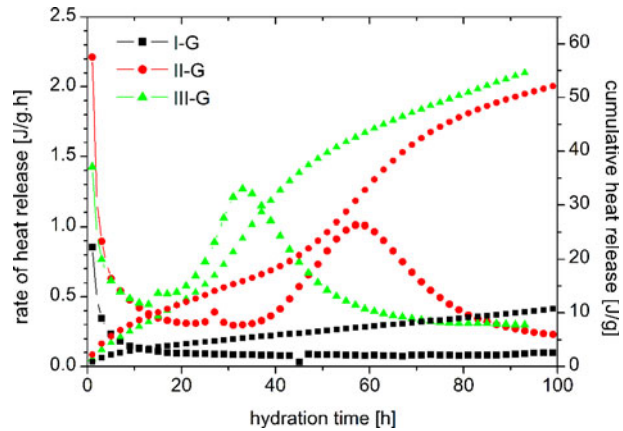


Fig. 11—Heat release during hydration of granulated slags.

respectively, could be assigned to the pre-induction period of hydration of the C_2S phase.

The curves of cumulative heat release illustrate that the higher the basicity of the material, the higher the heat release, although considerations in terms of absolute values should be performed on the basis of equal fineness of the powder. This is in good agreement with the XRD results where the amount of β - C_2S increased with an increase in basicity.

Figures 12(a) through (c) show the DTG (first derivatives of TGA) curves of all three hydrated slags after 3, 7, and 28 days of hydration. Four interesting areas can be pointed out on these curves. The part below 473 K (200 °C) is associated with dehydration of interlayer water of calcium silicate hydrates (C-S-H) as the main hydration product of hydrating β - C_2S .^[33] The area between 623 K and 693 K (350 °C and 420 °C) was associated with the weight loss resulting from the dehydration of brucite.^[33] Reactions in the temperature

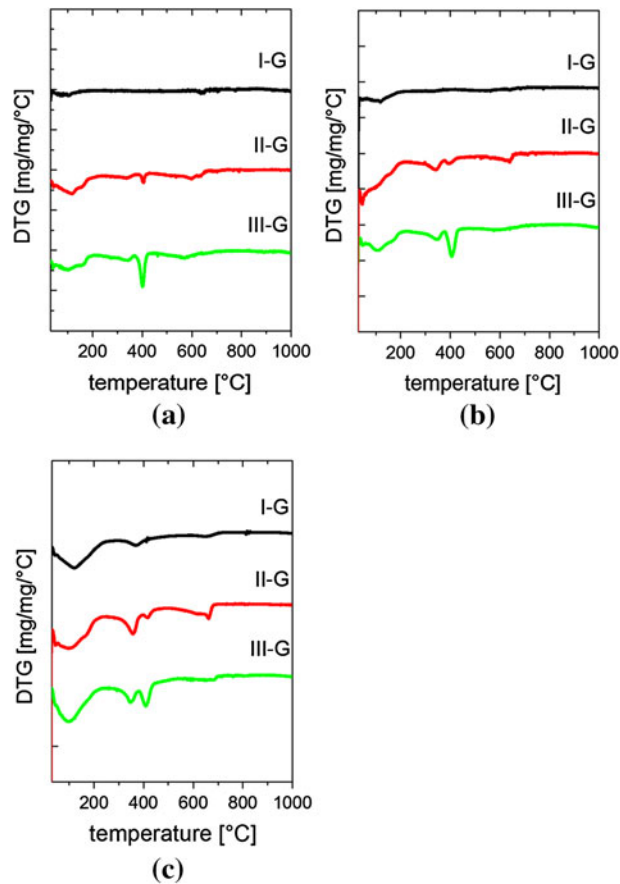


Fig. 12—DTG curves of hydrated slags after (a) 3 days, (b) 7 days and (c) 28 days of hydration.

range between 698 K to 823 K (425 °C to 550 °C) were primarily associated with the dehydration of $\text{Ca}(\text{OH})_2$ ^[34,35] and above 823 K (550 °C), partially due to the dissociation of carbonates associated with CO_2 release.

The progress of hydration during the first 28 days was clearly visible when comparing Figures 12(a) through (c). All three stabilized slags reacted with water and created hydration products such as $\text{Ca}(\text{OH})_2$, $\text{Mg}(\text{OH})_2$, and C-S-H. However, the hydration and formation of C-S-H phase was more pronounced for the slags with higher basicities as more $\beta\text{-C}_2\text{S}$ was present. The differences were evident in the rate of hydration as well. In particular, the early hydration during the first 7 days progressed significantly faster for slags with higher basicity. This indicates that the hydraulic reactivity was enhanced when more C_2S was present compared with the other phases. Indeed, merwinite, bredigite, cuspidine, and fluorite are considered to possess rather low hydraulic activity.^[36,37] Carbonated phases in the hydrated material, most likely CaCO_3 and MgCO_3 , were present probably due to the reaction with air during sample preparation.

SEM investigations on hydrated slags indicated that C-S-H gel was eventually formed in all three studied samples. The progress of hydration was mostly visible on slag III-G sample, and thus, only these results are presented in Figure 13. Slag III-G contained after granulation the highest amount of $\beta\text{-C}_2\text{S}$ and therefore

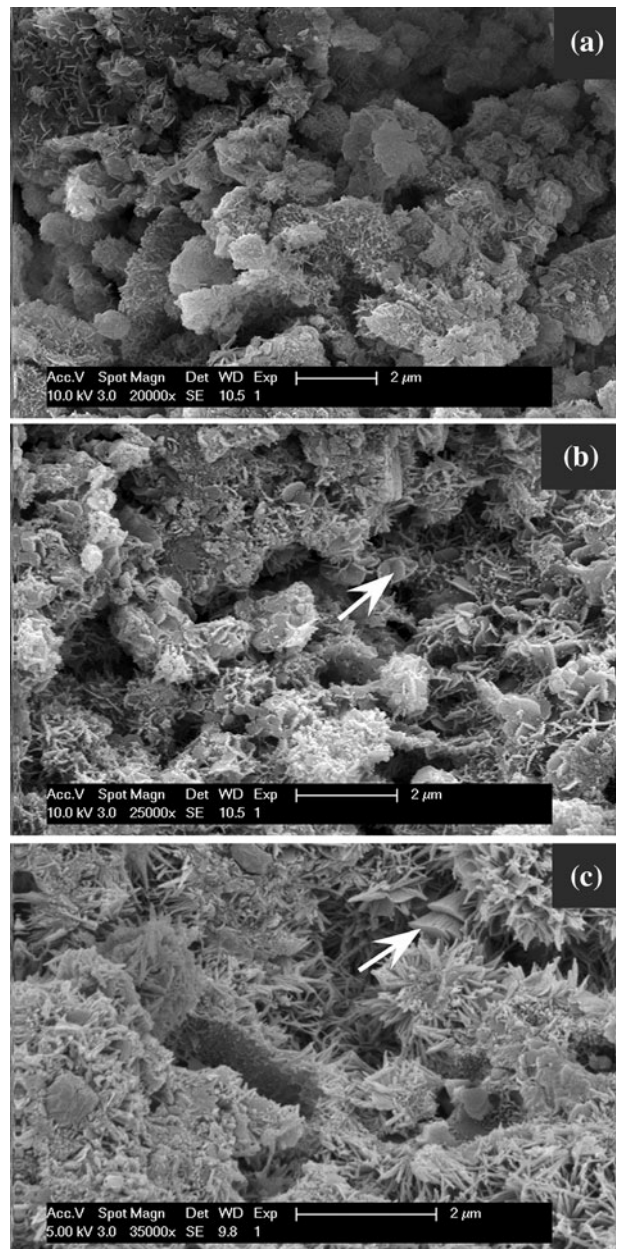


Fig. 13—SE micrographs of slag III-MS after (a) 3 days, (b), and (c) 28 days of hydration.

the hydration was more pronounced compared with the other studied slags. Flake-like C-S-H gel had already formed after 3 days of hydration, Figure 13(a). Original grains were still visible in the structure and the porosity was also relatively high. At 7 days of hydration the structure became significantly more compact, Figure 13(b). The gel filled up more of the space and CH hexagonal crystals were also visible (marked with arrow). After 28 days, the structure of the hydrated slag sample was rather dense, Figure 13(c). Well-developed acicular C-S-H crystals were present and the original slag grains were not visible any longer. Some CH and brucite crystals (marked with arrow) were present as well. These micrographs correspond well with the DTG results, where the peak at less than 473 K (200 °C) was

present after 7 days and did not change significantly afterward.

IV. CONCLUSIONS

The main conclusions are summarized as follows:

1. Both methods of high cooling rate for solidification, *i.e.*, granulation and water quenching, may lead to volume stabilization of synthetic stainless steel slags with various basicities.
2. Cooling rate calculations showed that water quenching was slower during the first 0.2 seconds compared with granulation, but because water is a much more efficient cooling medium than air, the average temperature of the granules dropped faster at later times with respect to granulation. The developed model for the heat transfer identified the thickness of the cooled material as the main governing parameter of the overall cooling rate.
3. C_2S , merwinite, and bredigite are the major phases in the solidified slags. The amount of C_2S increases as the basicity of the slag raises.
4. FactSage equilibrium calculations correspond well with the experimental data for slow cooling, and only minor deviations are observed. More differences were observed between calculation based on Scheil–Gulliver assumptions and rapidly cooled slag. These were mainly related to the bredigite phase which may form at sub-solidus temperatures and is thus not predicted by Scheil–Gulliver calculations.
5. The mineralogy of slags at RT subjected to rapid cooling by means of granulation and water quenching is rather similar for slags with the same basicity. The impact of cooling rate is substantial when slow (furnace) and fast cooling methods are compared.
6. Granulated slags show hydraulic reactivity, which is more pronounced in slag with higher basicity, in view of the higher β - C_2S content. The main hydration products are C-S-H, $Ca(OH)_2$, and $Mg(OH)_2$.
7. This article showed that the rapid cooling appears to be a promising way to stabilize the stainless steel slag and change it into a higher value product which could be further utilized as a hydraulic binder.

ACKNOWLEDGMENTS

The authors gratefully acknowledge the financial support from Aperam and IWT O&O Project 090594. Y. Pontikes and Ö. Cizer are thankful to the Research Foundation—Flanders for the post-doctoral fellowship.

REFERENCES

1. T.A. Engh, C.J. Simensen, and O. Wijk: *Principles of Metal Refining*, Oxford University press, Oxford, 1992.
2. C. Shi and S. Hu: *Cem. Concr. Res.*, 2003, vol. 33, pp. 1851–56.

3. G.H. Thomas and I.M. Stephenson: *Silic. Ind.*, 1978, vol. 43, pp. 195–200.
4. S.N. Gosh, B. Rao, A.K. Paul, and K. Raina: *J. Mater. Sci.*, 1979, vol. 14, pp. 1554–66.
5. G.W. Grooves: *J. Mater. Sci.*, 1983, vol. 18, pp. 1615–24.
6. C.J. Chan, W.M. Kriven, and J.F. Young: *J. Am. Ceram. Soc.*, 1992, vol. 75, pp. 1621–27.
7. A. Seki, Y. Aso, M. Okubo, F. Sudo, and K. Ishizaka: *Kawasaki Steel Gihō*, 1986, vol. 18, pp. 20–24.
8. G.-C. Lai, T. Nojiri, and K.-I. Nakano: *Cem. Concr. Res.*, 1992, vol. 22, pp. 743–54.
9. Y.-M. Kim and S.-H. Hong: *J. Am. Ceram. Soc.*, 2004, vol. 87, pp. 900–05.
10. Y. Pontikes, P.T. Jones, D. Geysen, and B. Blanpain: *Arch. Metall. Mater.*, 2010, vol. 55, pp. 1167–72.
11. M. Tossavainen, F. Engstrom, Q. Yang, N. Menad, M. Lidstrom Larsson, and B. Bjorkman: *Waste Manag. (Oxford)*, 2007, vol. 27, pp. 1335–44.
12. M. Barati, S. Esfahani, and T.A. Utigard: *Energy*, 2011, vol. 36, pp. 5440–49.
13. G. Li: *Proc. 1st Int. Slag Valorization Symp.*, Leuven, BE, 2009. pp. 165–76.
14. C.W. Bale, P. Chartrand, S.A. Degterov, G. Eriksson, K. Hack, R. Ben Mahfoud, J. Melançon, A.D. Pelton, and S. Petersen: *CALPHAD*, 2002, vol. 26, pp. 189–228.
15. D. Durinck, P.T. Jones, B. Blanpain, P. Wollants, G. Mertens, and J. Elsen: *J. Am. Ceram. Soc.*, 2007, vol. 90, pp. 1177–85.
16. L. Gan, C. Zhang, F. Shangguan, and X. Li: *Metall. Mater. Trans. B*, 2012, vol. 43B, pp. 460–67.
17. P.T. Jones, D. Desmet, M. Guo, D. Durinck, F. Verhaeghe, J. Van Dyck, J. Liu, B. Blanpain, and P. Wollants: *J. Eur. Ceram. Soc.*, 2007, vol. 27, pp. 3497–507.
18. Y. Kashiwaya, T. Nakauchi, K.S. Pham, S. Akiyama, and K. Ishii: *ISIJ Int.*, 2007, vol. 47, pp. 44–52.
19. K.I. Draznevski, A.M. Mullis, and R.F. Cochrane: *Mater. Sci. Eng. A*, 2004, vols. 375–377, pp. 485–87.
20. L. Pandelaers, F. Verhaeghe, P. Wollants, and B. Blanpain: *Int. J. Heat Mass Transf.*, 2011, vol. 54, pp. 1039–45.
21. R.B. Bird, W.E. Stewart, and E.N. Lightfoot: *Transport Phenomena*, Wiley, New York, 2002.
22. Y.-Z. Zhao, Y.-H. Zhao, Q. Li, S.-L. Chen, J.-Y. Zhang, and K.-C. Chou: *Intermetallics*, 2009, vol. 17, pp. 491–95.
23. L.M. Juckes: *Miner. Process. Extr. Metall.*, 2002, vol. 111, pp. 120–28.
24. D. Moseley and F.P. Glasser: *Cem. Concr. Res.*, 1981, vol. 11, pp. 559–65.
25. G.W. Groves: *Cem. Concr. Res.*, 1982, vol. 12, pp. 619–24.
26. K.J. Neuvonen: *Heat of Formation of Merwinite and Monticellite*, Yale University, Yale, 1952.
27. Mindat.org. [23.11.2011]; Available from: <http://www.mindat.org/>.
28. PremierPericlase. *Unique Large Crystal Sintermagnesia from Premier Periclase*. [30.7.2012]; Available from: http://www.premierpericlase.com/docs/large_crystal_sintermagnesia_paper.pdf.
29. J.W. Anthony, R.A. Bideaux, K.W. Bladh, and M.C. Nichols: *Handbook of Mineralogy*. [30.7.2012]; Available from: <http://www.handbookofmineralogy.org/>.
30. D. Durinck: Ph.D. Thesis, KU Leuven, 2008.
31. F. Xiuji and L. Shizong: *Cem. Concr. Res.*, 1986, vol. 16, pp. 587–601.
32. D.L. Kantro and C.H. Weise: *J. Am. Ceram. Soc.*, 1979, vol. 62, pp. 621–26.
33. V.S. Ramachandran, R.M. Paroli, J.J. Beaudoin, and A.H. Delgado: *Handbook of Thermal Analysis of Construction Materials*, Noyes Publications, Norwich, 2002.
34. S. Kumar, A. Bandopadhyay, T.C. Alex, and R. Kumar: *Ceram. Int.*, 2006, vol. 32, pp. 555–60.
35. H.F.W. Taylor: *Cement Chemistry*, Academic Press, London, 1990.
36. Q. Yang, F. Engström, B. Björkman, and D. Adolfsson: *Proc. VIII Int. Conf. Molten Slags, Fluxes Salts*, 2009. pp. 33–41.
37. H. Alanyali, M. Çöl, M. Yilmaz, and S. Karagöz: *Int. J. Appl. Ceram. Technol.*, 2009, vol. 6, pp. 736–48.